Analyses of the power generation performance and the non-equilibrium plasma of a disk MHD generator

- **Le Chi Kien**

Ho Chi Minh City University of Technology and Education

(Manuscript Received on March 12nd, 2015, Manuscript Revised April 04th, 2016)

ABSTRACT

Recently, closed cycle MHD power generation system studies have been focused on improving the isentropic efficiency and the enthalpy extraction ratio. By reducing the cross-section area ratio of the disk MHD generator, it is believed that a high isentropic efficiency can be achieved with the same enthalpy extraction. In this study, the results relating to a plasma state which takes into account the ionization instability of non-equilibrium seeded plasma is added to the theoretical prediction of the relationship between enthalpy extraction and isentropic efficiency. As a result, the electron temperature, which reaches the seed complete ionization state without the growth of ionization instability, can be realized at a relatively high seed fraction condition. However, the upper limit of the power generation performance is suggested to remain lower than the value expected in the low seed fraction condition. It is also suggested that a higher power generation performance may be obtained by implementing the electron temperature range, which reaches the seed complete ionization state at a low seed fraction.

Key words: *Isentropic efficiency, enthalpy extraction, ionization instability, seed fraction, closed cycle MHD.*

1. INTRODUCTION

In recent years, closed cycle MHD power generation research has been placed on improving the isentropic efficiency in addition to the enthalpy extraction ratio with a great interest.

Enthalpy extraction ratio (*EE*) is defined as the ratio of the electrical output to the heat input while the isentropic efficiency (*IE*) is the ratio of $|h_i–h_f|_{\text{actual}}$ to $|h_i–h_f|_{\text{isentropic}}$. Here h_i, h_f represent the total enthalpy of the initial state and the final state respectively, and IE represents the ratio of the enthalpy change in case of extracting the enthalpy isentropically to the actual enthalpy change.

By reducing the cross-section area ratio of the disk MHD generator (generator channel horizontal outlet section area / throat cross-section area), a high *IE* can be achieved experimentally with the same *EE*. It is also predicted the relationship between *EE* and *IE* agrees with a simple theoretical study that using the generator channel cross-sectional area ratio and an outlet Mach number as variables in a small-scale MHD generator. Furthermore, from

the study of the relationship between the stagnation pressure and the power generation performance, the fluid machine characteristics is clearly revealed.

On the other hand, it is known that the affect of the state of non-equilibrium plasma used as a working fluid to the power generation performance is large, and the ionization instability that causes the spatial non-uniformity of the plasma is the main reason for the deterioration of power generation performance. This causes the effective decrease of Hall parameter and electrical conductivity.

In this study, the results relating to a plasma state which takes into account the ionization instability of non-equilibrium seeded plasma is added to the theoretical prediction of the relationship between *EE* and *IE* considering only in hydrodynamics. Thus, this study considers the plasma physical aspects that have not been sufficiently performed in the previous study [1], [2] for a generator with small cross-sectional area ratio. Here, instead of obtaining the numerical solutions of differential equations as in the conventional numerical simulation, a discussion based on the simple analytic steady local calculations has been carried out. The purpose is to further develop the analytical consideration on the power generation performance.

2. ANALYSIS METHOD

2.1 Electron energy transfer

Non-equilibrium plasma is composed of noble gas Argon atoms, argon ions, seed Cesium atoms, Cesium ions, and electrons. The temperatures of Argon atoms, Argon ions, Cesium atoms, Cesium ions (T_g) are equal. Only the electron temperature T_e is different ($T_e > T_g$) and a two-temperature model is used [3],[4]. In the non-equilibrium seeded plasma generated in the disk-shaped MHD generator, the Joule heating is shown below and the energy transfer due to the collision are balanced in the steady local state.

From the generalized Ohm law, the Joule heating, which has an effect of increasing the electron energy, becomes the following equation.

$$\frac{|\boldsymbol{j}|^2}{\sigma_{eff}} = \frac{\sigma_{eff}}{1+\beta_{eff}^2} u_r^2 B^2 \left(1+\beta_{eff}^2 K_h^2\right) \qquad (1)$$

Here, $\boldsymbol{E}=(E_r, 0, 0)$ is an electric field strength vector, $\boldsymbol{u}=(u_r, 0, 0)$ is the flow velocity vector, then the load factor K_h defined as $K_h \equiv |E_r/\beta_{eff} u_r B|$. $\boldsymbol{j}$, B is the current density vector and the constant magnetic flux density to be applied to the vertical direction of the flow (r-θ-z coordinate system). The effective electrical conductivity σ_{eff} and the effective Hall parameter β_{eff} will be explained in the next section.

The energy loss of electrons by collision A is shown by the following equation

$$A = 3\kappa m_e n_e \left(T_e - T_g\right) \sum_h^{heavy} \frac{\overline{\upsilon}_{eh}}{m_h} \qquad (2)$$

Here κ, m_e, n_e is the Boltzmann constant, electron mass, electron number density, $\overline{\upsilon}_{eh} = n_h \overline{c}_e \overline{Q}_{eh}$, h indicates the heavy particles, n_h is the h particle number density, $\overline{Q}_{eh}$ is the average momentum transfer collision cross-section between h particle and electron, $\overline{c}_e = \left(8\kappa T_e/\pi m_e\right)^{1/2}$ is the average thermal velocity of electron.

The electron energy equation balanced by Eq. (1) and (2) can be solved analytically for T_e, therefore by using T_e as a variable, the solutions on plasma quantities can be achieved.

In this paper, the collision phenomenon of power generation plasma will be described. Here, the effect of elastic collisions in the form of Eq. (2), including the effects of inelastic collisions as ionization process described below, is taken into

account. However in this case, because the change of T_g is considered very small with respect to the change of T_e, T_g is kept constant. Furthermore, because the local in the mainstream of plasma fluid is a study object, the energy flow to the wall is not considered.

Although there are various processes in the ionization and recombination phenomena of plasma, they are in a balanced state in the MHD generator plasma, meaning that the ionization equilibrium is assumed. This means the Saha equation representing the equilibrium conditions on ionization is used, and the electron number density is calculated in a plasma with the local thermal equilibrium. In this case, the state equations of perfect gas are used.

2.2 Critical Hall parameter

In the linear theory on ionization instability of non-equilibrium MHD power generation plasma, the growth rate of small disturbances is considered, and the stability condition of the plasma which the disturbances do not grow is found out [3],[5]. Here, the critical Hall parameter β_{cr} have been defined.

$$\beta_{cr} = \left(\frac{A_T^2 - \sigma_T^2}{n_T^2} \right)^{1/2} \tag{3}$$

$$A_T = \frac{T_e}{A}\frac{dA}{dT_e},\ \sigma_T = \frac{T_e}{\sigma}\frac{d\sigma}{dT_e},\ n_T = \frac{T_e}{n_e}\frac{dn_e}{dT_e}$$

Plasma will be stable under the condition that the Hall parameter β does not exceed β_{cr}. In this study, β_{eff} and σ_{eff} are determined as [6]

$\beta_{cr} \geq \beta$:

$$\beta_{eff} = \beta = eB/m_e\bar{\upsilon}_e \tag{4}$$

$$\sigma_{eff} = \sigma = e^2 n_e / m_e\bar{\upsilon}_e \tag{5}$$

$\beta_{cr} < \beta$:

$$\beta_{eff} = \beta_{cr} \tag{6}$$

$$\sigma_{eff} = \frac{\beta_{cr}}{\beta}\sigma \tag{7}$$

By using the β_{eff} and σ_{eff}, the effective quantities of non-equilibrium MHD seeded plasma that takes into account the ionization instability in the analytical calculation can also be represented. In other words, the Hall parameter and the spatial non-uniformity of electrical conductivity are difficult to analyze at the present time but they will become apparent from the measurement, and when estimating their effective values this calculation, to some degree, is expected to agree with. Thereafter, the Hall parameters and electrical conductivity that do not take into account the ionization instability are described as the β and σ to distinguish from the effective values.

2.3 Enthalpy extraction and isentropic efficiency

The enthalpy extraction (*EE*) is represented by the following equation.

$$1 - EE = \left(\frac{p_{0e}}{p_{0i}} \right)^{\frac{\eta_p(\gamma-1)}{\gamma}} = \ldots \tag{8}$$

$$\ldots = \left[\left(\frac{A_t}{A_e}\frac{1}{M_e} \right)^{\frac{\gamma-1}{\gamma}} \left(\frac{2+(\gamma-1)M_e^2}{\gamma+1} \right)^{\frac{\gamma+1}{2\gamma}} \right]^{\frac{1}{\frac{1}{\eta_p}+\frac{1-\gamma}{2\gamma}}} \tag{9}$$

Here p_{0e}, p_{0i}, γ, A_t, A_e and M_e are the outlet total pressure, the inlet total pressure, specific heat ratio, throat cross-sectional area, outlet cross-sectional area, and the outlet Mach number. In addition, the polytropic efficiency η_p is represented by the following equation using the local Mach number M, β_{eff}, K_h.

$$\eta_p = \frac{\beta_{eff}^2 K_h (1 - K_h)}{1 + \beta_{eff}^2 K_h + \frac{\gamma-1}{2} M^2 \left(1 + \beta_{eff}^2 K_h^2\right)} \tag{10}$$

The relationship of *EE* and *IE* is shown as follows

$$1-\frac{EE}{IE}=\left(\frac{p_{0e}}{p_{0i}}\right)^{\frac{\gamma-1}{\gamma}}=\ldots \quad (11)$$

$$\ldots=\left(\frac{A_t}{A_e}\frac{\sqrt{1-EE}}{M_e}\right)^{\frac{\gamma-1}{\gamma}}\left(\frac{2+(\gamma-1)M_e^2}{\gamma+1}\right)^{\frac{\gamma+1}{2\gamma}} \quad (12)$$

The plasma fluid expands isentropically from a stagnation point state of p_{0i}=0.21MPa, total temperature T_0=2500K, and the analytical calculation is carried out with respect to the plasma state in the local that has reached a certain Mach number *M*. However, the magnetic flux density in the experiment attenuates smoothly (nonlinearly) 0.3T in the vicinity of the generator channel outlet along the disk radial direction when *B*=3T at the disk generator center position. In this paper, the flux density in the channel radial middle flow area where the power generation MHD interaction is considered relatively large to act sufficiently is assumed typical values, and use *B*=2T as calculation condition. By using η_p obtained from the Eq. (10), the *EE* is determined by Eq. (9) and relates to the *IE* by Eq. (12).

2.4 Calculation method

A splitting scheme is applied to the governing system with the subsets of equations describing different physical processes being solved in sequence by appropriate program modules. The MHD system is solved by the generalized TVD Lax-Friedrichs scheme which was developed for the unstructured mesh applications. A general monotonous reconstruction of mesh-defined functions is designed taking into account the dependence on two variables. For the case of a regular triangulation, this scheme ensures the second order approximation to spatial derivatives (the third order is possible with a special choice of the anti-diffusion limiters). The time integration is explicit, the second approximation order is reached due to the predictor – corrector procedure. The time step is restricted by the Courant criterion. The predictor and corrector steps are organized similarly but the numerical fluxes differ due to the different reconstruction of the functions. Namely, a nonmonotonic piecewise-linear continuous interpolation is used for the predictor, and special monotonic discontinuous reconstruction is created for the corrector. Thus, the corrector scheme not only improves the time-advance resolution but also appears to be a stabilizing procedure. For the solution of parabolic equations describing the conductive heat transfer, the author developed the finite-volume schemes constructed by analogy with mixed finite element method.

The electron energy transfer is described by the equation for spectral radiation intensity. Practical calculations are done via multigroup spectral approximation. The author solves the electron transport equation by means of semi-analytical characteristic algorithm. The analytical solution along the characteristic direction is constructed by means of the backward-forward angular approximation to the photon distribution function. The two-group angular splitting gives an analytical expression for radiation intensity dependent on opacity and emissivity coefficients. The energy exchange between radiation field and the gas is taken into account via a radiative flux divergence, which is incorporated into the energy balance as a source function.

The governing Critical Hall parameter set of equations is solved numerically employing a fully implicit finite difference method. To obtain the correct solutions of this method, the MHD equations have to be rewritten into conservation form, and the numerical scheme also has to be conservative. Numerical schemes used in computational MHD are Lax-Wendroff scheme

with artificial viscosity, finite differences with artificial viscosity, flux corrected transport, finite elements, spectral elements, discontinuous Galerkin. Furthermore, numerical diffusion can produce magnetic reconnection even in an ideal MHD model and the energy conservation will be violated by a non-conservative ideal MHD scheme because Joule heating is neglected. However, we should note that the reconnection is not very well modeled either by ideal or by resistive MHD. One needs to include more physics in MHD disk generator and/or go to really high grid resolution so that small scale instabilities can develop.

3. RESULTS AND DISCUSSION

Here the description of the static pressure in the channel and the outlet Mach number measurement is referred in [1],[2], and the spectroscopic measurement of electron temperature is performed by a multi-channel spectrometer [7]. In this case, the exposure time of 50μs is set up to detect a sufficiently strong light. On the other hand, the staying time of the fluid in the generator is about 150μs. Thus, T_e in this study has a meaning as average values with respect to time and space, therefore, it is impossible to get the local T_e corresponding to the small plasma structures that may be present in the generator.

3.1 Plasma stability

In order to examine the plasma stability and the relationship between *EE* and T_e, the T_e dependence of σ, σ_{eff}, β, β_{cr}, β_{eff}, and *EE* is shown in Fig. 1(a,b,c). The calculation conditions are *SF* (seed fraction) =2×10^{-4}, M=1.7, M_e=1.7.

As seen from the figure (a), the ionization of cesium atom is mainly accelerated when $2000 \leq T_e \leq 4350$K, and because the degree of ionization increases with the increase of T_e, σ increases. When $T_e \approx 4350$K, σ reaches 250S/m. The β from Fig. (b) decreases when T_e increases and it can be higher than 7 when T_e<3500K. Thus, the σ and β that do not take into account the ionization instability is not a primary factor that Cesium weakly ionized plasma state degrades the power generation performance.

On the other hand, from the calculation which takes into account the ionization instability, the β_{cr} that shows the ionization instability affect causing the Cesium weak ionization is very low when $2000 \leq T_e \leq 4350$K. For this reason, β_{eff} and σ_{eff} greatly decrease. The solution of *EE* that reflects the plasma state of extremely low β_{eff} and σ_{eff} does not exist (Fig. 1(c)). This result, by the steady local calculation, introduces the affect of ionization instability, and indicates that the spatial non-uniformity of plasma can be used to consider, to some extent, the affect to the power generation performance.

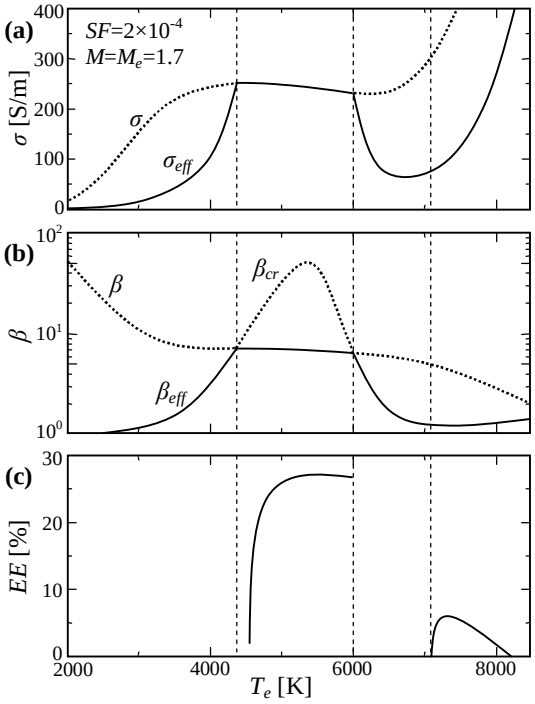

Figure 1. Relationship of Te and electrical conductivity (a), Hall parameter (b), enthalpy extraction (c)

When T_e is 4650K to 6000K, the plasma is considered as a state that Cesium is almost completely ionized while Argon is nearly not ionized. In the seed complete ionization state, ionization degree of plasma matches the ionization degree of Cesium, and σ_{eff} is nearly independent of T_e. As shown in Figs. 1(a,b), the large β_{cr}, the high β_{eff} of 7 as well as the σ_{eff}=230~250S/m can be realized. The large β_{cr} means that the plasma stability is high and the plasma is more uniform. Since the highest *EE*=28% is obtained when T_e=5500K, the realization of the seed complete ionization state is a useful condition for the high power generation performance (see Fig. 1(c)).

On the other hand, in the $T_e \geq 6000$K which accelerated not only Cesium but also the Argon ionization, β_{cr} is greatly reduced with the rise of T_e. This indicates that the ionization instability, which causes the Argon partial ionization, is occurred. Particularly when T_e is 6000~7100K, since β_{eff} as well as σ_{eff} is very low, the *EE* can not be solved.

When T_e is 7100~8200K as shown in Fig. 1(a), the relatively high $\sigma_{eff} \geq 75$S/m is obtained. Furthermore, although β_{cr} is less than β, the difference between the two is small compared to the difference found in $T_e \leq 4350$K as shown in Fig. 1(b). This suggests that the affect of ionization instability is relatively small. Therefore, there is a solution of *EE* even when T_e is high. However in this case *EE* is less than 6%, and this value is low as compared to the value obtained in the seed complete ionization state.

The above results have suggested that the plasma state varies greatly depending on the change of T_e and that state is a significant effect on the power generation performance.

3.2 Seed fraction

The dependence of seed fraction (*SF*) on the electron temperature T_e is described experimentally in [8] and shown in Fig. 2. The channel load resistance R_L, in this case, is 0.13Ω, 0.2Ω, 0.3Ω. However, the affect of load resistance value is not much, therefore, this paper focuses only on the change of *SF*.

From the figure, T_e of 7300~8100K can be obtained when the *SF*=2~4×10^{-4}. In addition, there is a decreasing trend of T_e (T_e=4700~5500K) when *SF* increases to 6~7×10^{-4}. When SF is 9~10×10^{-4}, the temperature T_e becomes 4800~5100K.

From the MHD generation theory, the *SF* of 2~4×10^{-4} has been suggested as a condition that the plasma fluid is expanded isentropically from the stagnation point state in the supersonic nozzle, and the Mach number of 1.7 at the nozzle outlet (or the MHD channel inlet) can be designed. On the other hand, a strong Lorentz force caused by the MHD interaction in the vicinity of the nozzle outlet works in the condition of 6~9×10^{-4}, so the fluid has a large deceleration.

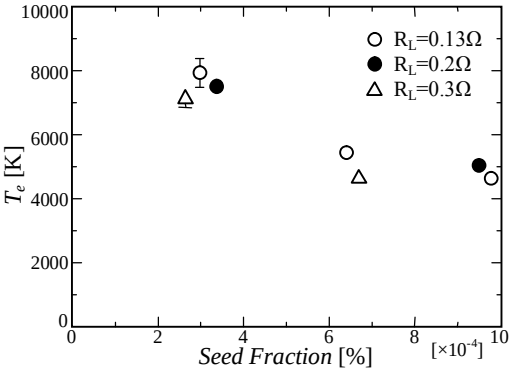

Figure 2. Relationship of Te and seed fraction

The increasing of *SF* increases the σ_{eff} of plasma and has the effect of accelerating Joule heating. Moreover, as the σ_{eff} increasing, the Lorentz force acting on the fluid becomes stronger and this causes a rise in static pressure which increases the energy loss due to the collisions and the reduction in flow speed that leads to the decreasing of induced electromotive

force. T_e of plasma is determined by the balance of both effects. The dependence of *SF* on T_e in Fig. 2, as well as the setting value of SF, indicates that this is one of the main factors to control the plasma state.

Figure 3 shows the dependence of (a) *EE*, (b) β_{eff}, (c) σ_{eff} on T_e when the SF is changed in the range 2×10^{-4}~9.5×10^{-4}. Here from the fluid behavior, the calculation conditions of $M=M_e=1.7$ for $SF=2$~4×10^{-4} and $M=M_e=1.1$ for $SF=6.5\times10^{-4}$ or 9.5×10^{-4} are given. In addition, the plot points (○,△,▲) in the same Fig. 3(a) is the experimental value referred in [8].

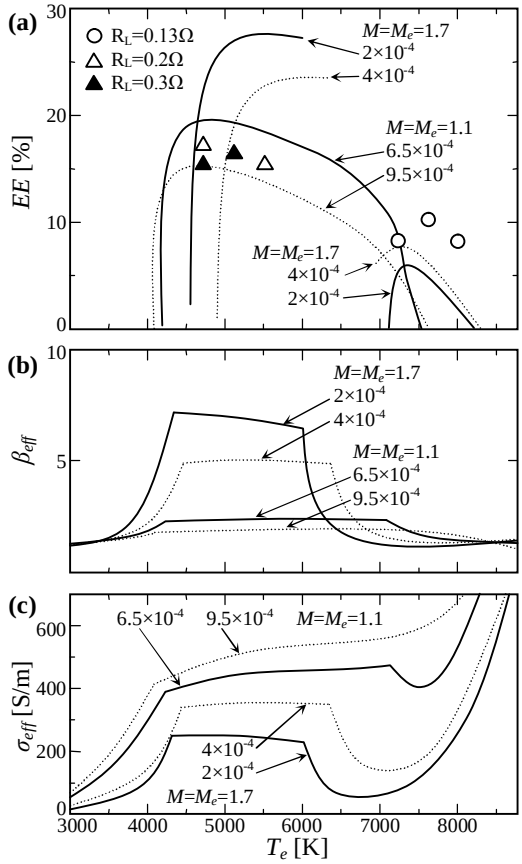

Figure 3. Calculated electron temperature Te

From the calculation results with the condition of $SF=2\times10^{-4}$ shown in Fig. 3(a), it can be seen that the solution of *EE* is obtained only in the range of T_e=4560~6000K and 7100~8200K. Similarly, *EE* is solved discontinuously only in the range of T_e=4900~6300K and 6900~8300K with the condition of $SF=2\times10^{-4}$.

Firstly, the calculated results are considered to compare with the experimental results when the range of T_e is more than 6500K. The ionization instability due to Argon weak ionization may occur in the case of $T_e\geq$6500K, and from the calculation, in this case, it is considered that β_{eff} is very low (nearly 1) as shown in Fig. 3(b). Here, the highest value of *EE* is as low as 6% and 8% when *SF* is 2×10^{-4} and 4×10^{-4} respectively. *EE* is also obtained relatively low value of 7~12% from the experiment in [8]. However, there is a trend that the calculated value is slightly higher than the experimental value. The cause of the difference between these two values can be explained that the value of *M* depends on the condition. In other words, there is a possibility that the experimental flow speed is higher than the calculated flow speed is given by the condition of M=1.7.

Next, the range of T_e=4600~6300K is considered. From the calculation, $\sigma_{eff} \geq$ 200S/m can be obtained even in the low *SF* condition, and a very high *EE* can be expected because a sufficient β_{eff} is maintained. However, that power generation performance is not obtained experimentally. This is because the temperature T_e which implements a seed complete ionization state cannot be achieved experimentally at a low *SF*.

From the calculation results with $SF=6.5$~9.5×10^{-4} in Fig. 3, it is seen that the discontinuity does not appear in the *EE*–T_e curve because the dependence of T_e on β_{eff} is relatively small. In addition, the *EE* obtained from the calculation in the range T_e= 4600~4700K is maximum, and this maximum value tends to decrease from 19% to 15% with the increase of *SF*. In this case, the obtaining of *EE* is considered independent from low β_{eff} to some extent because

the σ_{eff} is very high. The phenomenon that *EE* decreases with the increase of *SF* is because β_{eff} decreases with the increase of the collision frequency while σ_{eff} increases with the increase of *SF* in the seed complete ionization state. The decrease of β_{eff} reduces the electrical conversion efficiency η_p, therefore, *EE* decreases.

As shown in Fig. 2 under the condition of SF=6.5~9.5×10^{-4}, T_e reaches 4500~5500K and the seed complete ionization state is implemented. In this case, as suggested by Fig. 3, it is believed that an appropriate σ_{eff} can be achieved with a high *SF*, and a relatively high power generation performance is also obtained. With the condition of SF=6.5×10^{-4} and 9.5×10^{-4}, the *EE* calculated here and the *EE* from reference [8] agree well. This suggests that the plasma is stable as discussed from the calculation in the case of T_e implementing the seed complete ionization.

3.3 Plasma state

Fig. 4 shows the *IE–EE* relationship obtained from the calculation with a typical *SF*. Since the measured M_e is in the range from 1.1 to 1.7, this relationship described by a theoretical curve of Eq. (12) is illustrated by the dotted line with A_e/A_t=4.25, M_e=1.1 and 1.7. Figure (b) shows the calculated contour lines of T_e on the *IE–EE* relationship with calculation conditions of SF=3×10^{-4}, M=1.7, M_e=1.1 and 1.7, and Fig. (c) with calculation conditions of SF=9.5×10^{-4}, M=1.1, M_e=1.1 and 1.7.

From the theoretical curve in Figs. 4(a,b,c), it is shown that there is an achievable *EE* with the condition that supersonic flow is maintained (M_e=1.1~1.7). The ratio of the *EE* and *IE* follows the macro hydrodynamic behavior. From Fig. 4(a) when increasing the *SF*, *IE* and *EE* increase. It is understood that the inclination *IE*/*EE* both values formed in this case may not deviate greatly the nearly linear slope by a given M_e.

As already discussed in the previous section, the power generation performance can be best when implementing the seed complete ionization plasma. The calculation results in Figs. 4(b,c) also indicate the highest power generation performance according to the conditions of *SF* and *M* when implementing the seed complete ionization plasma of T_e=4500~5500K.

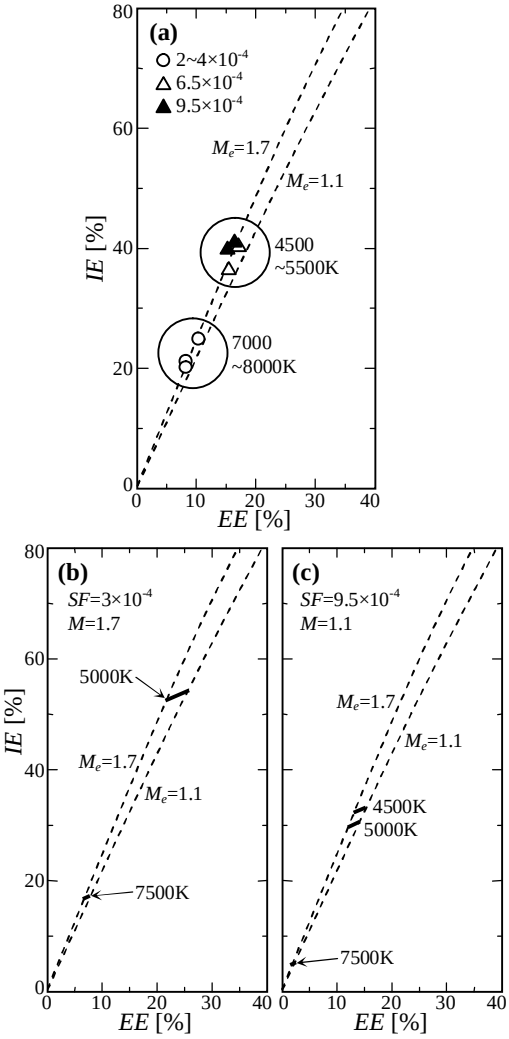

Figure 4. Relationship of isentropic efficiency and enthalpy extraction

More properly, when carrying out a power generation, which decelerates as much as possible (M_e=1.1) the supersonic flow, the highest *EE* and *IE* are realized. Therefore, it can

be said that these calculation results have suggested an upper limit of the achievable power generation performance. Furthermore, when *M* decreases due to the high *SF*, it is understood that the upper limit of power generation performance is lower than the expected value in case of low *SF*, high *M* even when obtaining a seed complete ionization plasma.

The MHD power generation using non-equilibrium seeded plasma depends on the electron temperature and its characteristic is that the plasma behavior changes clearly by the seed partial ionization, seed complete ionization, and the noble gas weak ionization state. Thus, the calculation values of *IE*, *EE* (Figs. (b,c)) based on the experimental values of the seed fraction and electron temperature is somewhat agreed with the experimental results.

4. CONCLUSIONS

This paper has carried out the steady local analysis of non-equilibrium seeded plasma which takes into account the ionization instability and has added aspects relating to a plasma state in regard to performance prediction of the macro hydrodynamic side that considers the relationship of isentropic efficiency and enthalpy extraction. By the theory analysis, the analysis of power generation results was performed.

The electron temperature, which reaches the seed complete ionization state without the growth of ionization instability, can be realized at a relatively high seed fraction condition. At this time, the high enthalpy extraction and isentropic efficiency are achieved. As a result, the electrical conductivity with small effective Hall parameter can be high, and a high power generation performance is suggested with the conditions of low Mach number, high seed fraction. However, the upper limit of the power generation performance, which is considered to be achievable at a high seed fraction, is suggested to remain lower than the value expected in the low seed fraction condition, simultaneously.

On the other hand, since the electron temperature increases to the Argon weak ionization state in the small seed fraction experiment, the power generation performance is low. From the analysis result, it is suggested that a higher power generation performance may be obtained by implementing the electron temperature range, which reaches the seed complete ionization state at a low seed fraction. By adding the affect of ionization instability, the plasma state in the experiment can be predicted by a steady local calculation, and a study of power generation performance based on this can be carried out.

Phân tích đặc tính phát điện và plasma không cân bằng của máy phát điện Từ thuỷ động loại đĩa

- **Lê Chí Kiên**

Trường Đại học Sư phạm Kỹ thuật TP.HCM

TÓM TẮT

Những nghiên cứu về hệ thống phát điện Từ thuỷ động gần đây đã tập trung vào việc cải thiện hiệu suất đoạn nhiệt và tỉ chiết enthalpy. Với việc giảm tỉ số mặt cắt ngang của máy phát điện Từ thuỷ động loại đĩa, hiệu suất đoạn nhiệt cao có thể nhận được với cùng tỉ chiết enthalpy. Trong bài báo này, những kết quả liên quan đến trạng thái của plasma mà có xét đến sự bất ổn định ion hoá của plasma cấy không cân bằng sẽ bổ sung vào dự đoán mang tính lý thuyết về quan hệ giữa tỉ chiết enthalpy và hiệu suất đoạn nhiệt. Kết quả là nhiệt độ của điện tử mà đạt đến trạng thái ion hoá hoàn toàn chất cấy mà không làm tăng sự bất ổn định ion hoá đã được xác định tại điều kiện tỉ số cấy khá cao. Tuy nhiên, giới hạn trên của đặc tính phát điện được đề nghị giữ thấp hơn kỳ vọng ở điều kiện tỉ số cấy thấp. Đặc tính phát điện cao hơn cũng có thể nhận được bằng cách tăng dải nhiệt độ điện tử đến trạng thái ion hoá hoàn toàn chất cấy ở tỉ số cấy thấp.

Từ khóa: *Hiệu suất đoạn nhiệt, tỉ chiết enthalpy, bất ổn định ion hoá, tỉ số cấy, MHD chu trình kín.*

REFERENCES

[1]. S.M. Aithal, Characteristics of optimum power extraction in an MHD generator with subsonic and supersonic inlets, *Energy Conversion and Management*, 50, 3, 765-771 (2009).

[2]. M.H. Saidi, A. Montazeri, Second law analysis of a magnetohydrodynamic plasma generator, *Energy*, 32, 9, 1603-1616 (2007).

[3]. S.M. Aithal, Shape optimization of an MHD generator based on pressure drop and power output constraints, *International Journal of Thermal Sciences*, 47, 6, 778-786 (2008).

[4]. Avrilios Lazaros, Experimental evidence and theory for the interaction of superthermal electrons with the MHD modes during ECRH, *Fusion Engineering and Design*, 53, 1-4, 35-42 (2001).

[5]. Y.A. Kholodov, A.S. Kholodov, E.L. Stupitzki, A.Y. Repin, Numerical simulation of the convective plasma dynamics stage at the ionosphere motion by means of 3D MHD equations, *Computer Physics Communications*, 164, 1-3, 91-97 (2004).

[6]. Shinji Takeshita, Chainarong Buttapeng, Nob. Harada, Characteristics of plasma produced by MHD technology and its application to propulsion systems, *Vacuum*, 84, 5, 685-688 (2009).

[7]. Juan Pablo Trelles, S. Mahnaz Modirkhazeni, Variational multiscale method for nonequilibrium plasma flows, *Computer Methods in Applied Mechanics and Engineering*, 282, 87-131 (2014).

[8]. Yiwen Li, Yinghong Li, Haoyu Lu, Tao Zhu, Bailing Zhang, Feng Chen, Xiaohu Zhao, Preliminary experimental investigation on MHD power generation using seeded supersonic Argon flow as working fluid, *Chinese Journal of Aeronautics*, 24, 6, 701-708 (2011).